Research Article | Vol. 8, No. 6 | 1 Jun 2018 | OPTICAL MATERIALS EXPRESS 1603
Optical Materials EXPRESS

Exposure dependence of the UV initiated optical absorption increase in polymer films with a soluble CdS precursor and its relation to the photoinduced nanoparticle growth

ANTON A. SMIRNOV,[1] ANDREY AFANASIEV,[1] SERGEY GUSEV,[2] DMITRY TATARSKIY,[2,3] NICKOLAI ERMOLAEV,[1] AND NIKITA BITYURIN[1,*]

[1]*Institute of Applied Physics of the Russian Academy of Sciences, 46 Ul'yanov Street, 603950 Nizhny Novgorod, Russia*
[2]*Institute of Physics of Microstructures of the Russian Academy of Sciences, 603950 Nizhny Novgorod GSP-105, Russia*
[3]*N.I. Lobachevsky State University of Nizhny Novgorod, 23 Gagarin Ave, 603950 Nizhny Novgorod, Russia*
** bit@ufp.appl.sci-nnov.ru*

Abstract: Evolution of the UV-induced absorption within the polymer matrix possessing a highly soluble CdS precursor is studied. The initially optically transparent (polymethylmethacrylate based) samples are irradiated by a light-emitting diode operated at 365 nm for different intensities and different temperatures. In situ monitoring of the process is performed at a wavelength of 405 nm where the samples are initially transparent. The study shows that the increase in absorbance is temperature dependent, and at a fixed temperature it is determined by UV exposure rather than the intensity or irradiation time separately. TEM, HR TEM data, as well as data on absorption and luminescent spectra, allow the relation of the optical absorption evolution to the CdS nanoparticles growth process. This provides new valuable information on the kinetics of this phenomenon in UV irradiated polymer films with a soluble precursor.

OCIS codes: (160.4236) Nanomaterials; (160.4760) Optical properties; (160.5335) Photosensitive materials; (350.3850) Materials processing; (350.4990) Particles; (350.5130) Photochemistry.

References and links

1. N. M. Bityurin, "Laser Nanostructuring of Polymers," in *Fundamentals of Laser–Assisted Micro- and Nanotechnologies*, V. P. Veiko, V. I. Konov, eds. (Springer International Publishing, Switzerland, 2014).
2. A. Alexandrov, L. Smirnova, N. Yakimovich, N. Sapogova, L. Soustov, A. Kirsanov, and N. Bityurin, "UV initiated growth of gold nanoparticles in PMMA matrix," Appl. Surf. Sci. **248**(1–4), 181–184 (2005).
3. A. Athanassiou, R. Cingolani, E. Tsiranidou, C. Fotakis, A. M. Laera, E. Piscopiello, and L. Tapfer, "Photon-induced formation of CdS nanocrystals in selected areas of polymer matrices," Appl. Phys. Lett. **91**(15), 153108 (2007).
4. F. Antolini, A. Ghezelbash, C. Eposito, E. Trave, L. Tapfer, and B. A. Korgel, "Laser-induced nanocomposite formation for printed nanoelectronics," Mater. Lett. **60**(8), 1095–1098 (2006).
5. D. Fragouli, A. M. Laera, G. Caputo, V. Resta, P. P. Pompa, L. Tapfer, R. Cingolani, and A. Athanassiou, "The effect of polymer matrices in the in-situ CdS formation under UV irradiation of precursor-polymer films," J. Nanosci. Nanotechnol. **10**(2), 1267–1272 (2010).
6. D. C. Onwudiwe, T. P. J. Krüger, and C. A. Strydom, "Laser assisted solid state reaction for the synthesis of ZnS and CdS nanoparticles from metal xanthate," Mater. Lett. **116**, 154–159 (2014).
7. N. Bityurin, A. Alexandrov, A. Afanasiev, N. Agareva, A. Pikulin, N. Sapogova, L. Soustov, E. Salomatina, E. Gorshkova, N. Tsverova, and L. Smirnova, "Photoinduced nanocomposites—creation, modification, linear and nonlinear optical properties," Appl. Phys., A Mater. Sci. Process. **112**(1), 135–138 (2013).
8. F. Stellaci, C. A. Bauer, T. Meyer-Friedrichsen, W. Wenseleers, V. Alain, S. M. Kuebler, S. J. K. Pond, Y. Zhang, S. R. Marder, and J. W. Perry, "Laser and electron-beam induced growth of nanoparticles for 2D and 3D metal patterning," Adv. Mater. **14**(3), 194–198 (2002).
9. A. K. Bansal, M. T. Sajjad, F. Antolini, L. Stroea, P. Gečys, G. Raciukaitis, P. André, A. Hirzer, V. Schmidt, L. Ortolani, S. Toffanin, S. Allard, U. Scherf, and I. D. W. Samuel, "In situ formation and photo patterning of emissive quantum dots in small organic molecules," Nanoscale **7**(25), 11163–11172 (2015).

#322597 https://doi.org/10.1364/OME.8.001603
Journal © 2018 Received 5 Feb 2018; revised 10 Apr 2018; accepted 8 May 2018; published 21 May 2018

Optical Materials EXPRESS

10. A. Camposeo, M. Polo, A. A. R. Neves, D. Fragouli, L. Persano, S. Molle, A. M. Laera, E. Piscopiello, V. Resta, A. Athanassiou, R. Cingolani, L. Tapfer, and D. Pisignano, "Multi-photon in situ synthesis and patterning of polymer-embedded nanocrystals," J. Mater. Chem. **22**(19), 9787–9793 (2012).
11. V. Resta, A. M. Laera, A. Camposeo, E. Piscopiello, L. Persano, D. Pisignano, and L. Tapfer, "Spatially confined CdS NCs in-situ synthesis through laser irradiation of suitable unimolecular precursor-doped polymer," J. Phys. Chem. C **116**(47), 25119–25125 (2012).
12. N. Sapogova, A. Pikulin, A. A. Smirnov, and N. Bityurin, "Diffusion-controlled alteration of inhomogeneous materials: tailoring of the spatial distribution of nanoparticles in nanocomposites," Phys. Chem. Chem. Phys. **18**(48), 32921–32930 (2016).
13. N. O. Yakimovich, N. V. Sapogova, L. A. Smirnova, A. P. Aleksandrov, T. A. Gracheva, A. V. Kirsanov, and N. M. Bityurin, "Gold-containing nanocomposition materials on the basis of homo-and copolymers of methylmethacrylate," Russ. J. Phys. Chem. B **2**(1), 128–134 (2008).
14. M. Alsawafta, S. Badilescu, A. Paneri, V.-V. Truong, and M. Packirisamy, "Gold-poly(methyl methacrylate) nanocomposite films for plasmonic biosensing applications," Polymers (Basel) **3**(4), 1833–1848 (2011).
15. E. Yilmaz and S. Suzer, "Au nanoparticles in PMMA matrix: In situ synthesis and the effect of Au nanoparticles on PMMA conductivity," Appl. Surf. Sci. **256**(22), 6630–6633 (2010).
16. Z.-B. Sun, X.-Z. Dong, W.-Q. Chen, S. Nakanishi, X.-M. Duan, and S. Kawata, "Multicolor polymer nanocomposites: In situ synthesis and fabrication of 3D microstructures," Adv. Mater. **20**(5), 914–919 (2008).
17. P. K. Khanna and N. Singh, "Light emitting CdS quantum dots in PMMA: synthesis and optical studies," J. Lumin. **127**(2), 474–482 (2007).
18. S. Scalbi, V. Fantin, and F. Antolini, "Environmental assessment of new technologies: Production of a quantum dots-light emitting diode," J. Clean. Prod. **142**(4), 3702–3718 (2017).
19. N. Bityurin, L. Znaidi, and A. Kanaev, "Laser-induced absorption in titanium oxide based gels," Chem. Phys. Lett. **374**(1–2), 95–99 (2003).
20. A. I. Kuznetsov, O. Kameneva, A. Alexandrov, N. Bityurin, P. Marteau, K. Chhor, C. Sanchez, and A. Kanaev, "Light-induced charge separation and storage in titanium oxide gels," Phys. Rev. E Stat. Nonlin. Soft Matter Phys. **71**(2 Pt 1), 021403 (2005).
21. O. Kameneva, A. Kuznestov, L. A. Smirnova, L. Rozes, C. Sanchez, A. Alexandrov, N. Bityurin, Ph. Marteau, and A. Kanaev, "New photoactive organic-inorganic materials based on titanium-oxo-PHEMA nanocomposites exchibiting mixed valence properties," J. Mater. Chem. **15**(33), 3380–3383 (2005).
22. A. I. Kuznetsov, O. Kameneva, L. Rozes, C. Sanchez, N. Bityurin, and A. Kanaev, "Extinction of photo-induced Ti^{3+} centres in titanium oxide gels and gel-based oxo-PHEMA hybrids," Chem. Phys. Lett. **429**(4), 523–527 (2006).
23. N. Agareva, A. A. Smirnov, A. Afanasiev, S. Sologubov, A. Markin, E. Salomatina, L. Smirnova, and N. Bityurin, "Properties of cadmium-(bis)dodecylthiolate and polymeric composites based on it," Materials (Basel) **8**(12), 8691–8700 (2015).
24. A. A. Smirnov, A. Afanasiev, N. Ermolaev, and N. Bityurin, "LED induced green luminescence in visually transparent PMMA films with CdS precursor," Opt. Mater. Express **6**(1), 290–295 (2016).
25. A. K. Bansal, F. Antolini, M. T. Sajjad, L. Stroea, R. Mazzaro, S. G. Ramkumar, K.-J. Kass, S. Allard, U. Scherf, and I. D. W. Samuel, "Photophysical and structural characterisation of in situ formed quantum dots," Phys. Chem. Chem. Phys. **16**(20), 9556–9564 (2014).
26. V. Resta, A. M. Laera, E. Piscopiello, M. Schioppa, and L. Tapfer, "Highly efficient precursors for direct synthesis of tailored CdS nanocrystals in organic polymers," J. Phys. Chem. C **114**(41), 17311–17317 (2010).
27. K. Hölz, J. Lietard, and M. M. Somoza, "High-Power 365 nm UV LED Mercury Arc Lamp Replacement for Photochemistry and Chemical Photolithography," ACS Sustain. Chem.& Eng. **5**(1), 828–834 (2017).
28. K. Ramasamy, M. A. Malik, M. Helliwell, J. Raftery, and P. O'Brien, "Thio- and dithio-biuret precursors for zinc sulfide, cadmium sulfide, and zinc cadmium sulfide thin films," Chem. Mater. **23**(6), 1471–1481 (2011).
29. C. F. Bohren and D. R. Huffman, *Absorption and Scattering of Light by Small Particles* (A Wiley-Interscience publication, John Wiley &Sons, New York, Chichester, Bribane, Totonto, Singapore, 1983).
30. L. E. Brus, "Electron–electron and electron-hole interactions in small semiconductor crystallites: The size dependence of the lowest excited electronic state," J. Chem. Phys. **80**(9), 4403–4409 (1984).
31. S. Ninomiya and S. Adachi, "Optical properties of wurtzite CdS," J. Appl. Phys. **78**(2), 1183–1190 (1995).
32. N. Bityurin, "UV etching accompanied by modifications. Surface etching," Appl. Surf. Sci. **138–139**, 354–358 (1999).
33. N. Bityurin, B. S. Luk'yanchuk, M. H. Hong, and T. C. Chong, "Models for laser ablation of polymers," Chem. Rev. **103**(2), 519–552 (2003).

1. Introduction

Self-assembly of the species originated from the light-induced precursor destruction can result in nanoparticle formation within the polymer matrix [1–7]. The optical properties of such photoinduced nanocomposites usually drastically differ from those of the initial materials. This provides an opportunity for patterning of the initially homogeneous material because the nanoparticles are formed only within the irradiated domains [7–11]. Another way

Optical Materials EXPRESS

to perform patterning is discussed in [12]. Here, the inhomogeneity in the spatial distribution of nanoparticles relies on the laser-induced inhomogeneity of the matrix properties.

The light-induced formation of gold or silver nanoparticles in materials of this kind has been studied for a decade [2,7,13–15]. Nanocomposites with photoinduced semiconductor nanoparticles, e.g., CdS, are also of interest because of their luminescent properties [16,17], which is promising for applications in light-emitting diode (LED) production technologies [18]. At the same time, the sufficiently large light-induced CdS nanoparticles have an effective absorption cross-section of about $2 \cdot 10^{-18}$ cm^2 per CdS unit within the optical range with $\lambda < 500$ nm. This cross-section value is close to that of such well-recognized strongly absorbing photoinduced species as Ti^{3+}centers in TiO_2 gel and TiO_2 gel-based organic-inorganic hybrids [19–22].

Most of the previously published papers used CdS precursors, which are not soluble in the polymer matrix. In this case, the nanoparticles are formed within the precursor islands in the matrix, and the process resembles the one occurring within the grains of powder [23]. Some good soluble CdS precursors have recently been reported [24–26]. This gives rise to the problem of studying and understanding of the particle formation mechanism in this case. Diffusion of species should play a significant role in the process. In the present paper, we study UV irradiation of polymer films with bis(1,1,5,5-tetraethyl-2,4-dithiobiureto)cadmium(II) [$Cd(N(SCNEt_2)_2)_2$] (TEDBCd) as a precursor. This compound is readily soluble in many organic solvents and could be a very promising candidate as a precursor for photoinduced nanocomposites with polymethylmethacrylate (PMMA) matrix, offering an opportunity to prepare visually transparent PMMA films with a precursor content of up to 10% [24]. Relatively cheap and easy-to-use ultraviolet light emitting diodes (UV LEDs) with a central wavelength of 365 nm [27] were chosen as light sources for this processing [24]. We employ transmission electron microscopy (TEM) and high-resolution TEM (HRTEM) to prove the formation of CdS nanoparticles within the samples under UV irradiation.

In the present paper, we designed a special setup allowing us to irradiate the samples at controlled temperatures and light intensities, and thereby to examine the effect of UV photons and temperature separately. We obtained a somewhat unexpected result. At a given temperature, the effect of UV radiation on the sample is determined by the exposure (doze) rather than the light intensity and irradiation time separately. This result may shed light on the mechanism of nanoparticle nucleation and growth in the photoinduced nanocomposites with soluble CdS precursors.

2. Sample preparation and UV irradiation

Cadmium complex TEDBCd was prepared as described in [28]. Then it was introduced into the PMMA matrix. Due to the high solubility of the precursor, the process of obtaining samples reduced to a simple casting of the toluene solution of the desired concentration on a fused silica substrate and drying at room temperature. In order to prevent liquid spreading on the surface and to fix the thickness of the film, the substrate was put into a specially designed fluoroplastic container. The resulting PMMA film is characterized by a high transparency in the visible region of the spectrum.

For the UV irradiation the sample was placed into a heater between two quartz windows transparent for UV light. A specially designed heater-thermostat provided a controlled temperature that was monitored with an Optris PI400 thermal imager (Optris GmbH, Germany). To make the measurement more accurate, we attached a special adhesive tape with known emissivity (Testo Inc., USA) on the window. UV irradiation was provided by LED NVSU233A (Nichia, Japan) with a central wavelength of 365 nm. UV light was turned on when the measured temperature was stabilized. The scheme of the experimental setup is presented in Fig. 1. We used the part of radiation not coming to the sample as a reference. Measuring the intensity of this reference part of the radiation with a spectrometer (QE65Pro,

Optical Materials EXPRESS

Ocean Optics, Dunedin, FL, USA) allowed us to determine the UV exposure of the sample (J cm^{-2}).

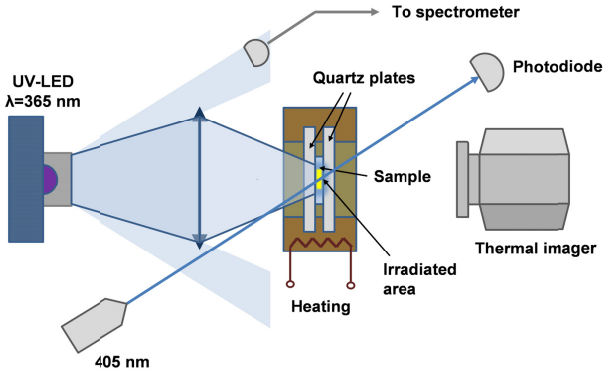

Fig. 1. Scheme of the setup for studying the kinetics of the photoinduced process.

3. Electron microscopy

The particle size and the crystalline structure of the nanoparticles formed in the irradiated areas were studied by means of transmission electron microscopy (TEM). TEM measurements were performed with a LIBRA 200 MC Schottky Field emission gun instrument (Carl Zeiss AG, Germany) operated at 200 kV and an information resolution limit of 0.12 nm. For TEM sample preparation, a drop of either treated or untreated (PMMA)/TEDBCd film solution in toluene was deposited over the surface of a KCl crystal with spin coating at ~2000 rpm and then was covered by carbon films with a thickness of about 15 nm. Usually the PMMA film thickness ranged from 100 to 200 nm. After that, the PMMA film was separated from the surface of salt in water and was deposited on a TEM grid. Taking into account that the particle size can be of the order of a few nanometers, for high resolution TEM measurements it was necessary to extract the particles from the PMMA matrix. For this purpose, the PMMA films on TEM grids were processed in a soft oxygen plasma using Evactron 25/45 De-Contaminating RF Plasma Cleaning System (XEI Scientific, Inc., USA). This processing is typically used to remove organic materials from the surface of the TEM samples. The plasma processing mode which we used provided dry etching of PMMA at a rate of ~1 nm min^{-1}. During the TEM studies we examined both plasma-treated and untreated structures. The TEM images were acquired and processed with Digital Micrograph software (Gatan, Inc., USA).

For example, TEM micrographs of the PMMA/TEDBCd sample with a precursor mass fraction of 5% are presented in Fig. 2 for the non-irradiated (Fig. 2(a)) and LED-irradiated (Fig. 2(b),(c)) cases. The bright field (BF) micrographs of the initial samples (prior to irradiation) show the contrast which is typical of amorphous carbon and PMMA films (Fig. 2(a)). Upon irradiation, on micrographs we observe individual particles and clusters of several nanoparticles, which are visible as dark and light dots on the BF and the dark field (DF) images correspondingly. The presence of the PMMA and carbon film reduces the contrast and affects the quality of the TEM images. Nevertheless, the CdS nanocrystals are clearly visible in the TEM micrographs of PMMA /CdS films after the UV irradiation. Unfortunately, the evaluation of the CdS particle size distribution in nanocomposites is rather difficult due to the assembling and aggregation of the nanocrystals. However, by carrying out a comparative analysis of BF and DF images of the same area of the composite film we estimated the dimensions of the CdS nanocrystals. For example, Fig. 2(d),e shows histograms of the particle size distributions for the PMMA/TEDBCd sample with a precursor mass fraction of 5% and irradiated with an UV exposure of 2.3 kJ cm^{-2} (2 h, 320 mW cm^{-2}) at 110 °C obtained

Optical Materials EXPRESS

by processing of BF (Fig. 2(d)) and DF (Fig. 2(e)) images. First of all, the width of the distributions is relatively large and indicates that the QDs are not monodispersed. Secondly, the difference between the average particle sizes obtained from BF and DF images is obvious. This difference is caused by the fact that on the BF image we observe both isolated particles and their clusters of several pieces. From the DF image, we determine the average size of crystallites (coherently diffracting domains), and this is a more accurate characteristic of the size of CdS nanoparticles.

The high-resolution (HR) micrographs, in which the crystal lattice of the nanoparticles was clearly visible, permitted use to assess more accurately their size and conclude about the presence of a particular crystalline phase (Fig. 2(f),(g)). The observed particles have lattice constants $d_1 \approx 0.36$ nm and $d_2 \approx 0.316$ nm, which corresponds to lattices (100) and (101) of hexagonal CdS form. Also, from these images we can see that the apparent sizes of these crystallites are in good agreement with the sizes of the coherent scattering domains, which is observed in the DF images.

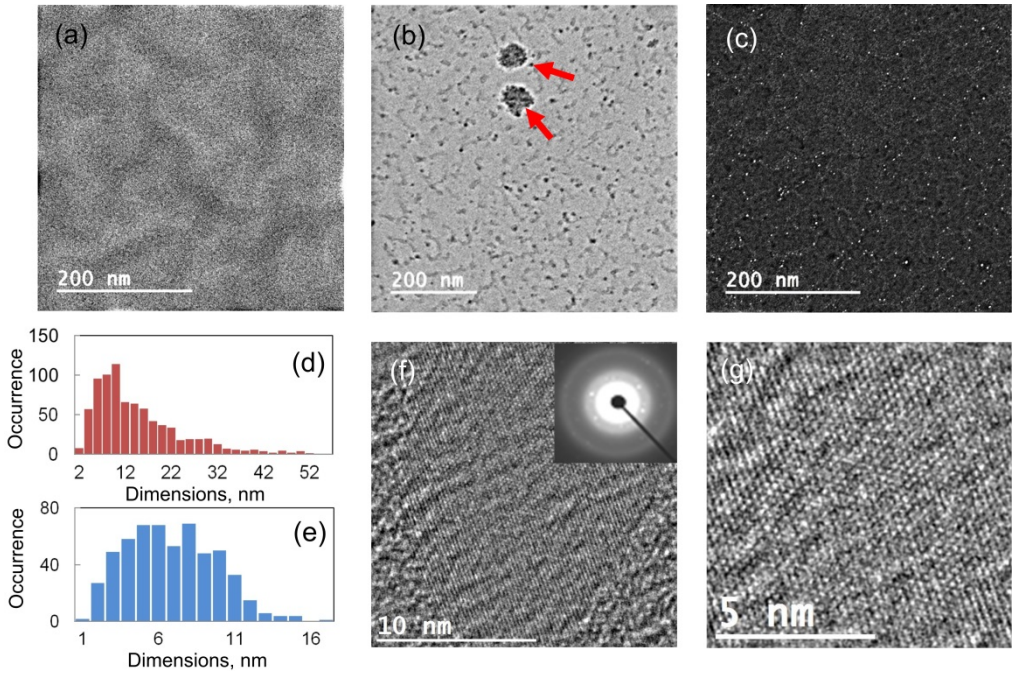

Fig. 2. TEM micrographs of the PMMA/TEDBCd thin films with a precursor mass fraction of 5% as is in (a) and irradiated with UV exposure 2.3 kJ cm^{-2} (2 h, 320 mW cm^{-2}) at 110 °C (b,c). The nanoparticles are seen as dark spots on the BF image (b), and bright dots on DF image (c). The clusters of these nanoparticles are marked by arrows. (d,e): Histograms of the particles sizes for PMMA/TEDBCd sample obtained from BF (d) and DF (e) images. (f,g): HRTEM micrographs of CdS nanoparticles in the irradiated PMMA/TEDBCd film. The inset shows the NanoBeam electron diffraction patterns of the corresponding cluster.

3. UV processing of samples and study of their optical properties

For a detailed study of the UV-induced process, we used PMMA films with a thickness of about 200 μ and a TEDBCd mass fraction of 5%. We performed UV irradiation of the film samples at three different measured temperatures, namely, 90 °C ± 2°C, 100 °C ± 2°C, and 110 °C ± 2°C. At these values, no damage or bubble formation for the sample occurred.

The UV light intensity in the LED-irradiated spot was about 400 mW cm^{-2}. This value slightly varied during the experiment due to the LED heating. For irradiation with reduced intensity, we employed a colored filter with a transmission of about 57% of the LED light without a sufficient transformation of its spectrum.

Optical Materials EXPRESS

For *in situ* monitoring of the nanoparticle growth process, we measured the absorbance of the irradiated sample at a wavelength of 405 nm. The sample initially is transparent at this wavelength.

Figure 3(a) demonstrates the evolution of the absorbance at 405 nm during the UV irradiation process for different cases. It is clear from the plot that for a given temperature the optical properties of the irradiated sample mainly depend on the integrated exposure. After the irradiation, we measured the full absorbance spectrum of the samples using a Shimadzu UV-1800 spectrophotometer. It is also shown that at different intensities the same exposure provides the same absorbance spectrum (see Fig. 3(b)). It can be seen that all the absorbance vs. exposure curves are close to linear starting from some incubation exposure (see Fig. 3(c)).

The results can be qualitatively understood within the framework of a simplified model. Analysis of Mie theory expansion of the extinction cross section for small-size CdS nanoparticles shows that for nanoparticle diameters of the order of 10 nm the absorption term [29]

$$\sigma_{abs} = \frac{8\pi^2 n_m}{\lambda} a^3 \frac{3\varepsilon'' \varepsilon_m}{\left(\varepsilon' + 2\varepsilon_m\right)^2 + \varepsilon''^2} \tag{1}$$

strongly dominates the other terms, including the scattering one. Here, a is the radius of the particle, n_m and ε_m are the refractive index and dielectric constant of the matrix, and ε' and ε'' are the real and imaginary parts of the dielectric constant of the bulk CdS at the wavelength λ. The above formula shows that if the quantum confinement is not significant, that is, if the radii of nanoparticles are large enough, then the absorption cross section is proportional to the volume of the nanoparticle or the number of CdS units within it.

This means that the input of the growing CdS nanoparticles into the absorption coefficient of the sample at a wavelength of 405 nm is approximately proportional to the number density of the CdS units aggregated within relatively large nanoparticles.

On the contrary, the sufficiently small CdS nanoparticles do not absorb at this wavelength because of the quantum confinement. The estimation [30] shows that the interband (valent zone – conduction zone) absorption at a wavelength of 405 nm is significant for nanoparticles larger than 4 nm in diameter. It takes some time for such nanoparticle to grow. The absence of the nanoparticles of this size in the beginning of the process should result in incubation (delay time between the start of the irradiation and the start of the absorption elevation) seen in Fig. 3(c).

We relate the growth of absorption at a wavelength of 400 nm and larger with the CdS units accumulation within the nanoparticles. The estimations based on the known bulk optical constants [31] see Fig. 4 and Eq. (2) from Appendix, yield a value about $5 \cdot 10^{-18}$ cm^2 for the effective absorption cross section per CdS unit. The destruction of the precursor molecule can be accompanied by the formation of absorbing by-products. A priori, we cannot exclude this effect. However, the existence of a delay time in the absorption increase shows that the parasitic by-product absorption does not dominate.

Luminescent spectra of the irradiated films (see Fig. 3(d)) correspond to the spectra of CdS nanoparticles. It should be noted that luminescence is very sensitive to the surface condition of a nanoparticle, so that we can speak here only about a qualitative correspondence. Nevertheless, it is expedient to assume that the maximum of the luminescent signal is close to the bandgap wavelength of the CdS bulk materials. Moreover, it should be taken in consideration that the bandgap of luminescent particles is somewhat larger than the bulk bandgap due to the quantum confinement.

Optical Materials EXPRESS

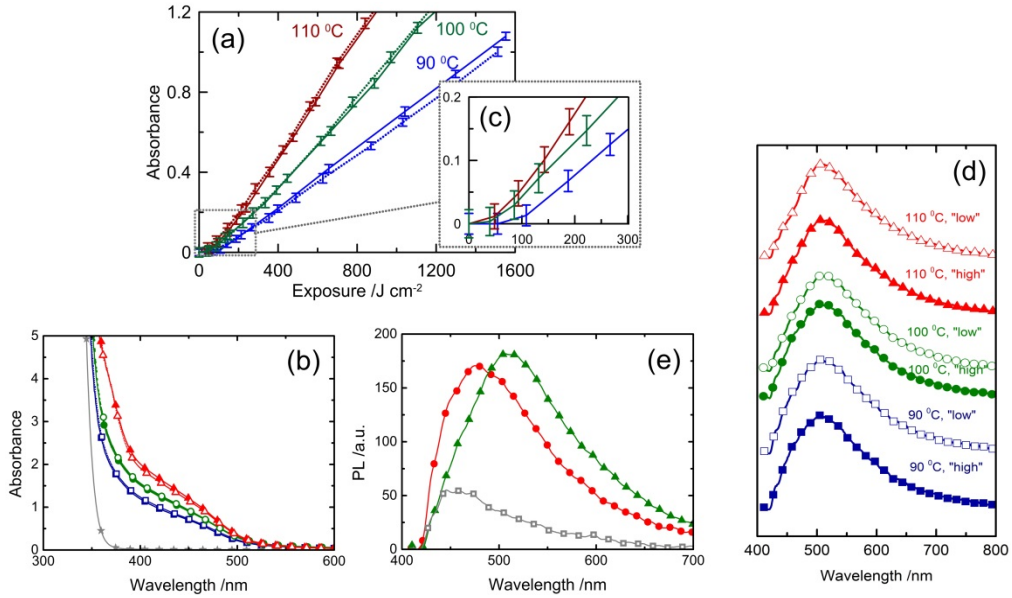

Fig. 3. (a) Absorbance at 405 nm vs UV exposure for the PMMA/TEDBCd film with a precursor mass fraction of 5% for three different temperatures (90 °C, 100 °C, and 110 °C) and two optical power densities: "high" (about 400 mW cm^{-2}) – solid lines and "low" (57% of high passing through the glass filter) – dotted lines. (b) Absorbance spectra of the PMMA/TEDBCd film with a precursor mass fraction of 5% irradiated with an UV exposure of 1.5 kJ/cm^2 under three different temperatures, namely, 90 °C (blue lines, squares), 100 °C (green lines, circles), and 110 °C (red lines, triangles). The spectra for the samples irradiated with "high" intensity are presented as solid lines with filled symbols; for "low" intensity – dotted lines with empty symbols. The spectrum of the non-irradiated sample is shown by a gray line with star symbols. (c) Magnified plot for small exposures at high intensity. (d) Normalized PL spectra of the PMMA/TEDBCd film with a precursor mass fraction of 5% irradiated with UV exposure 1.5 kJ/cm^2 under three different temperatures (90 °C, 100 °C, and 110 °C). The spectra for the samples irradiated with "high" intensity are presented filled symbols; for "low" intensity – with empty symbols. (e) PL spectra of the PMMA/TEDBCd film with a precursor mass fraction of 5%: non-irradiated (gray curve, empty squares), irradiated for 3 min (75 J/cm^2 exposure) at 100 °C (red curve, filled circles), irradiated with an UV exposure of 1.5 kJ/cm^2 for 1 hour at 100 °C (green curve, filled triangles). The excitation wavelength is 405 nm.

Evolution of the luminescent spectra at small exposures indicates a shift of the maximum of the luminescent spectrum towards the longer wavelengths (Fig. 3(e)). This agrees with the particle growth process.

Within the frame of the simplified model of light absorption of nanoparticles of different sizes, knowing the data on absorbance spectra and on the optical constants of CdS (Fig. 4(a)), it is possible to reconstruct the size distribution of nanoparticles absorbing light within the range of 400-500nm (see Appendix). The results show that there is quite a broad distribution of nanoparticles with different sizes up to 8-10nm (see Fig. 4(b)). Qualitatively, it corresponds to the distribution of Fig. 2(e). The shift from small towards large nanoparticle sizes in Fig. 2(e) comparing to the distribution in Fig. 4(b) can be explained by the aggregation of nanoparticles occurring within the solution.

The photoinduced formation of CdS nanoparticles is a complicated process that includes a photo-mediated destruction of the precursor molecules followed by a diffusion-assisted growth of nanoclusters. The above results (see Fig. 3) can be understood as suggesting that the precursor destruction is the limiting stage here. For the description of the absorbance evolution, the approach to mathematical modeling of the bulk photochemical processes considered in, e.g., Ref. 32 and in Ch. II A of Ref. 33 can be applied with some coefficients,

Optical Materials EXPRESS

e.g., a temperature-dependent quantum yield. The modeling is beyond the scope of the present paper and will be published elsewhere.

It is important that the above process of precursor destruction and particle growth cannot be separated in time, as it is, e.g., with $HAuCl_4$ as a gold precursor [2]. To prove this statement, we performed thermal annealing of samples at 90 °C irradiated previously at room temperature. In this case, the change in optical properties is insignificant in comparison with the UV irradiation at elevated temperature.

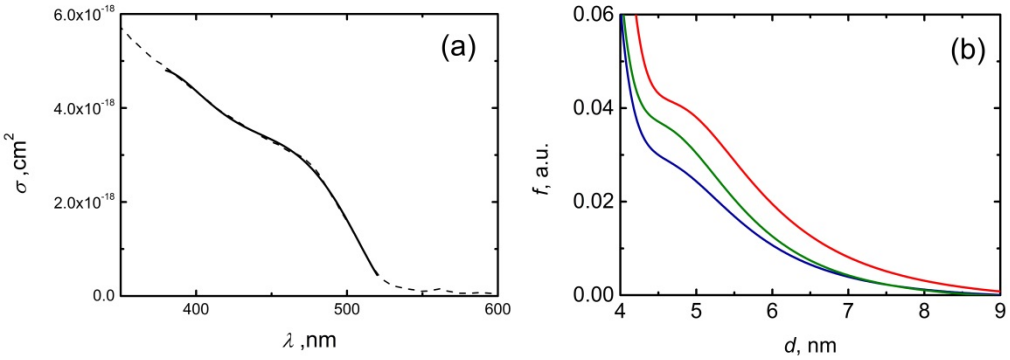

Fig. 4. (a) Absorption cross-section per single CdS unit according to Mie theory (dashed line) calculated using the averaged data on optical constants of CdS published in [31] and fifth-order fit (solid line). (b) Particle size distribution functions (arbitrary units) corresponding to optical absorbance at wavelength range 400-500nm (see Appendix) for different temperatures: 90 °C (blue line), 100 °C (green line), and 110 °C (red line).

4. Conclusions

Within this paper, we have studied the combined effect of heating and UV irradiation on the TEDBCd/PMMA samples. We clarify both of these effects separately by performing the UV irradiation with different intensities and at different temperatures and following the kinetics of induced optical absorption. The TEM electronic microscopy proves the existence of CdS nanoparticles within the irradiated domains. Analysis of the UV induced absorption and luminescence spectra suggests that the evolution of the UV absorption is significantly affected by the CdS nanoparticle growth. Our study shows that at a given temperature and at different intensities, the result is determined by the integrated exposure. An increase in temperature increases the absorbance for the same exposure. The effect of annealing at elevated temperature of the sample irradiated at room temperature is insignificant compared with the effect of irradiation at elevated temperature. These data can be understood as suggesting that the limiting stage of the CdS nanoparticle nucleation and growth is the precursor photochemical destruction with temperature-dependent quantum yield.

Appendix

Let us consider the simplified model of optical absorption by CdS nanoparticles with some size distribution. Within this model, for each wavelength under consideration there are only two types of nanoparticles, namely, small ones, which are transparent, and large ones, for which the absorption cross-section can be estimated from (1) with the bulk dielectric constants. The wavelength dependence of the absorption cross-section (1) per single CdS unit yields

$$\sigma_B = \frac{18\pi}{\lambda} v_{CdS} \frac{n_m \varepsilon'' \varepsilon_m}{\left(\varepsilon' + 2\varepsilon_m\right)^2 + \varepsilon''^2}. \quad (2)$$

Here v_{CdS} is the volume per single CdS unit in the bulk material, $v_{CdS}=5\cdot10^{-23}$ cm^3.

Optical Materials EXPRESS

In what follows, we use the averaged values of the optical functions of hexagonal CdS from [31]. $\sigma_B(\lambda)$ is shown in Fig. 4(a).

The boundary size between absorbing and not absorbing nanoparticles can be estimated by means of a simple formula for the size dependence of the bandgap [30]

$$E_g(R) = E_{g0} + \frac{\pi^2\hbar^2}{2R^2}\left(\frac{1}{m_e^b} + \frac{1}{m_h^b}\right). \tag{3}$$

Here, m_e^b and m_h^b are the effective mass of the electrons and the holes within the bulk material, and R is the radius of the particle.

For each wavelength λ there is a boundary value of the nanoparticle radius $R(\lambda)$

$$R(\lambda) = \sqrt{\frac{\pi\hbar}{4c}\frac{1/m_e^b + 1/m_h^b}{1/\lambda - 1/\lambda_{gap}}}. \tag{4}$$

According to our model, if radius of a nanoparticle $r>R(\lambda)$, then the absorption cross section of each CdS unit within a nanoparticle does not depend on the nanoparticle size and is equal to $\sigma_B(\lambda)$ (2).

If we find the boundary value R^* for some particular wavelength λ^*, then the relation (4) for the other wavelengths can be overwritten

$$R(\lambda) = R^*\sqrt{\frac{\lambda_{gap}/\lambda^* - 1}{\lambda_{gap}/\lambda - 1}}. \tag{5}$$

From (5) one can express the boundary value of the wavelength, starting from which (for larger wavelengths) the nanoparticle of radius r cannot absorb

$$\bar{\lambda}(r) = \frac{\lambda_{gap}}{1 + (\lambda_{gap}/\lambda^* - 1)\left(R^*/r\right)^2}. \tag{6}$$

With the CdS constants (see [30]) and the data on the optical constants [31] taking λ^* = 405 nm, and λ_{gap} = 530 nm, we obtain R^* = 2 nm.

Within the considered model, the dependence of optical absorbance on the wavelength can be represented as

$$D(\lambda) = \int_{R(\lambda)}^{\infty} f(r)\frac{4\pi}{3v_{CdS}}r^3\sigma_B(\lambda)dr. \tag{7}$$

Here, *f(r)* is the size distribution function. Differentiating both parts of (7) with respect to the wavelength and taking into account that $\int_{R(\lambda)}^{\infty} f(r)\frac{4\pi}{3v_{CdS}}r^3 dr = \frac{D(\lambda)}{\sigma_B(\lambda)}$ yields the following expression for the size distribution function:

$$f(r) = \frac{\Psi\left(\bar{\lambda}(r)\right)}{\frac{4\pi}{3v_{CdS}}r^3}, \tag{8}$$

where

$$\Psi(\lambda) = D(\lambda)\frac{\frac{\partial\sigma_B(\lambda)}{\partial\lambda}\frac{1}{\sigma_B(\lambda)} - \frac{\partial D(\lambda)}{\partial\lambda}\frac{1}{D(\lambda)}}{\sigma_B(\lambda)\frac{\partial R(\lambda)}{\partial\lambda}}. \tag{9}$$

Optical Materials EXPRESS

Equations (8) and (9) provide the solution of the inverse problem of finding the particle size distribution knowing the wavelength dependence of the absorbance.

In order to differentiate the scattering experimental data, we approximate $D(\lambda)$ and $\sigma_B(\lambda)$ within the interval 380 nm < λ < 520 nm by polynomial functions of the fourth and the fifth orders, correspondingly.

The result of the size (diameter) distribution functions evaluation for three values of temperature is shown in Fig. 4(b).

Funding

Russian Science Foundation (14-19-01702).

Acknowledgments

The authors thank Mr. I. Lukichyov for help with the sample preparation. The facilities of the "Physics and technology of micro- and nanostructures" Center at the IPM RAS were used for the TEM analysis of the samples.